Stan P. Korzilius
Department of Mathematics and Computer Science,
Eindhoven University of Technology,
Eindhoven 5600 MB, The Netherlands
e-mail: s.p.korzilius@tue.nl

Arris S. Tijsseling
Department of Mathematics and Computer Science,
Eindhoven University of Technology,
Eindhoven 5600 MB, The Netherlands
e-mail: a.s.tijsseling@tue.nl

Zafer Bozkuş
Hydromechanics Laboratory,
Department of Civil Engineering,
Middle East Technical University,
Ankara 06800, Turkey
e-mail: bozkus@metu.edu.tr

Martijn J. H. Anthonissen
Department of Mathematics and Computer Science,
Eindhoven University of Technology,
Eindhoven 5600 MB, The Netherlands
e-mail: m.j.h.anthonissen@tue.nl

Wil H. A. Schilders
Department of Mathematics and Computer Science,
Eindhoven University of Technology,
Eindhoven 5600 MB, The Netherlands
e-mail: w.h.a.schilders@tue.nl

Modeling Liquid Slugs Accelerating in Inclined Conduits

In this article, we simulate traveling liquid slugs in conduits, as they may occur in systems carrying high-pressure steam. We consider both horizontal and inclined pipes in which the slug is accelerated by a suddenly applied pressure gradient, while at the same time, gravity and friction work in the opposite direction. This causes a steep slug front and an extended slug tail. The shapes of front and tail are of interest since they determine the forces exerted on bends and other obstacles in the piping system. The study also aims at improving existing one-dimensional (1D) models. A hybrid model is proposed that enables us to leave out the larger inner part of the slug. It was found that the hybrid model speeds up the two-dimensional (2D) computations significantly, while having no adverse effects on the shapes of the slug's front and tail. [DOI: 10.1115/1.4037716]

1 Introduction

The phenomenon of traveling liquid slugs in pipelines inevitably occurs in the process of rapid pipe emptying and filling operations [1], but is especially observed in piping systems that carry high-pressure steam. In power plants, for instance, electricity is produced by means of steam turbines. When such systems are shut down for maintenance or lack thermal insulation, steam condensates and accumulates in the lower sections of the system. The liquid slug that thus arises forms a potential danger when the system is reactivated. Due to the high velocity of the slugs, which can easily be over 40 m/s, serious impact forces are imposed when they hit obstacles like bends and (partly) closed valves. This may lead to severe damage to the piping system, its supports, and its direct environment when leakage is the result. Severe accidents with casualties have been scrutinized in the literature [2–6]. Reference [2] is recommended reading for anyone interested in condensation-induced waterhammer, and Ref. [5] reports a 2500 kg pipe blown away an unbelievable distance of 800 m. Several laboratory investigations have been undertaken [7–12] as well as theoretical modeling and numerical simulation [13–21] on the formation, evolution, and structural impact of liquid slugs. The severity of the impact depends on the velocity and length of the slug, and on the steepness of its front. This is investigated herein by means of two-dimensional (2D) SPH simulations in order to check the plane-front assumption adopted in one-dimensional (1D) models and to quantify the amount of holdup (liquid that is left behind). In particular, it is computed how liquid is pushed out of a dip and how the slug's front and tail develop in time in an inclined pipe before hitting a downstream bend. To reduce the computation times, a hybrid 1D-2D model is proposed which is most efficient for multiphase pipe flows with large regions of pure liquid.

2 Mathematical Model

We will simulate the traveling slugs as two-dimensional bodies. To that end, we consider the vertical cross section through the

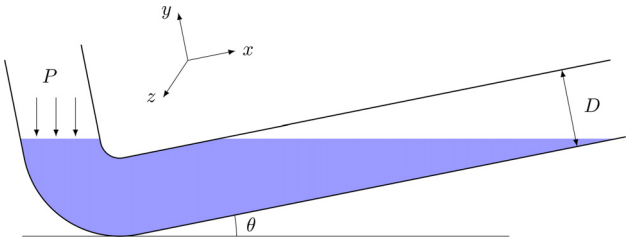

Fig. 1 A two-dimensional initial situation

Contributed by the Pressure Vessel and Piping Division of ASME for publication in the Journal of Pressure Vessel Technology. Manuscript received March 9, 2017; final manuscript received August 9, 2017; published online September 27, 2017. Assoc. Editor: Tomomichi Nakamura.

 Copyright © 2017 by ASME

central axis of the pipe, as depicted in Fig. 1. The x-axis is taken in the axial direction along the pipe. We neglect the effect of the circular shape of the pipe by assuming that there is no flow in the z-direction. In this way, we can directly use the continuity equation

$$\nabla \cdot \mathbf{v} = 0 \tag{1}$$

and the Euler equation

$$\frac{\mathrm{d}\mathbf{v}}{\mathrm{d}t} = \frac{-\nabla p}{\rho} + \mathbf{g} \tag{2}$$

to simulate the two-dimensional flow of the liquid. Notice that Eq. (2) implies that the fluid is assumed to be inviscid. The two-dimensional velocity vector $\mathbf{v}$ consists of the velocities u and v in the x and y-direction, respectively. The pressure is denoted by p, the density by ρ, and $\mathbf{g}$ is the gravitational acceleration vector.

Initially, the liquid is at hydrostatic rest. Then, as illustrated in Fig. 1, a constant pressure P is suddenly exerted on the left surface of the slug, while at the right surface, a zero gauge pressure is assumed. Skin friction at the pipe walls is included as an additional deceleration mechanism according to

$$\frac{\mathrm{d}u}{\mathrm{d}t} = -\frac{f}{2D}u^2 \tag{3}$$

where f is the Darcy–Weisbach friction coefficient and D is the hydraulic diameter of the circular and square conduits considered herein.

3 Numerical Method

3.1 Incompressible SPH (ISPH). We use smoothed particle hydrodynamics for our numerical simulations, in which the slug is described by a large number of incompressible particles, each of mass m. Every time step Δt (indicated by n), we carry out the following (more or less standard) calculations for each particle i:

- Compute the auxiliary velocity field resulting from gravity

$$\mathbf{v}_i^* = \mathbf{v}_i^n + \mathbf{g}\,\Delta t \tag{4}$$

- Compute the new pressure field from the Poisson equation

$$\langle \nabla^2 p_i \rangle^{n+1} = \frac{\rho}{\Delta t}\langle \nabla \cdot \mathbf{v}_i^* \rangle \tag{5}$$

- Calculate the new accelerations

$$\left\langle \frac{\mathrm{d}\mathbf{v}_i}{\mathrm{d}t} \right\rangle^{n+1} = \boldsymbol{\Gamma}_{i,\nabla}^{-1} \sum_{j \in S_i} m_j \left(\frac{p_j^{n+1} - p_i^{n+1}}{\rho_j \rho_i} \right) \nabla_{\mathbf{x}_j} K_{ij} \tag{6}$$

- Update the velocities

$$\mathbf{v}_i^{n+1} = \mathbf{v}_i^n + \left\langle \frac{\mathrm{d}\mathbf{v}_i}{\mathrm{d}t} \right\rangle^{n+1} \Delta t \tag{7}$$

- Update the particle positions

$$\mathbf{x}_i^{n+1} = \mathbf{x}_i^n + \frac{1}{2}\left(\mathbf{v}_i^n + \mathbf{v}_i^{n+1}\right)\Delta t \tag{8}$$

Here, S_i is the set of particles contained in the support domain of particle i, $K_{ij} := K(\mathbf{x}_i - \mathbf{x}_j, h)$ is a kernel function with smoothing parameter h, and $\boldsymbol{\Gamma}_{i,\nabla}$ is a normalization matrix defined by

$$\boldsymbol{\Gamma}_{i,\nabla} := -\sum_{j \in S_i} \nabla_{\mathbf{x}_j} K_{ij}\, \mathbf{x}_{ji}^{\mathrm{T}}\, V_j \tag{9}$$

where V denotes volume, $\mathbf{x}_{ji} := \mathbf{x}_j - \mathbf{x}_i$, and superscript T indicates transpose. The boundaries (both rigid walls and free surfaces) need special treatment, in that particles close to walls need to be mirrored in those walls and particles constituting the free surface need to be identified to impose the zero pressure boundary condition. Also, the flow separation points and the particle distribution require some attention, since without proper treatment particles will maneuver themselves into particle chains, thereby inevitably decreasing the accuracy. The precise details of the SPH algorithm used in this article are fully described in Ref. [22].

3.2 A Hybrid Model. The regions of particular interest are the front and the tail of the slug. These are the regions where genuine two-dimensional flow occurs. In the inner part of a slug in a straight pipe the velocities are unidirectional, with the magnitudes depending only on the y-coordinate. Despite its less interesting behavior, the inner part forms the largest part of the slug and therefore has a dominant contribution to the total computational effort. To make our algorithm more efficient—i.e., save computational time and avoid the need to store large matrices—we adopt a quasi two-dimensional model for the inner part of the slug. It turns out that the only assumption we need to include is that the pressure field inside the inner part is linear in the axial direction. The model is applicable only when the entire inner slug is in a straight section. It is a novel procedure and therefore fully described in Appendix A.

Results of the hybrid model are compared with those of the full simulation. To that end, we simulate an initially block-shaped slug of length $L_0 = 2\,\mathrm{m}$ and density $\rho = 1000\,\mathrm{kg/m^3}$, traveling in a horizontal pipe with diameter $D = 0.1\,\mathrm{m}$. The slug is accelerated by a suddenly applied upstream pressure of $P = 500{,}000\,\mathrm{Pa}$, and there is no friction with the walls. The particles are initially distributed hexagonally, with particle distance $d = 0.005\,\mathrm{m}$. This gives a total of 9223 particles. When the hybrid model is applied, the computations are started with only 1564 particles (representing front and tail), reducing the computational time by a factor 5. We emphasize, however, that this factor increases significantly when the liquid slug is much longer (for example, in pipe emptying), since this would increase the number of particles in the full simulation, while exactly the same number of particles can be used for a simulation with the hybrid model.

Figure 2 shows the tail of the slug at $t = 0.25\,\mathrm{s}$ for both the full simulation and the simulation that employs the hybrid model. If one looks closely, it is possible to distinguish slight variations in particle positions, but otherwise the shapes of the free surfaces are practically identical. Figure 3 confirms that the shapes and positions of the slug fronts are nearly the same.

3.3 Wall Friction. Wall or skin friction is caused by the fluid being in contact with the wall. Hence, the main contribution to the total amount of wall friction comes from the inner part of the slug. With the hybrid model, however, the inner part of the slug does not explicitly take part in the SPH computations. We therefore have to impose the effects of wall friction after the accelerations of the fluid particles in the front and tail of the slug have been computed. The average speed of the inner slug particles is

$$u_{\mathrm{avg}} = \frac{1}{|S|}\sum_{s \in S} \sqrt{\mathbf{v}_s^n \cdot \mathbf{v}_s^n} \tag{10}$$

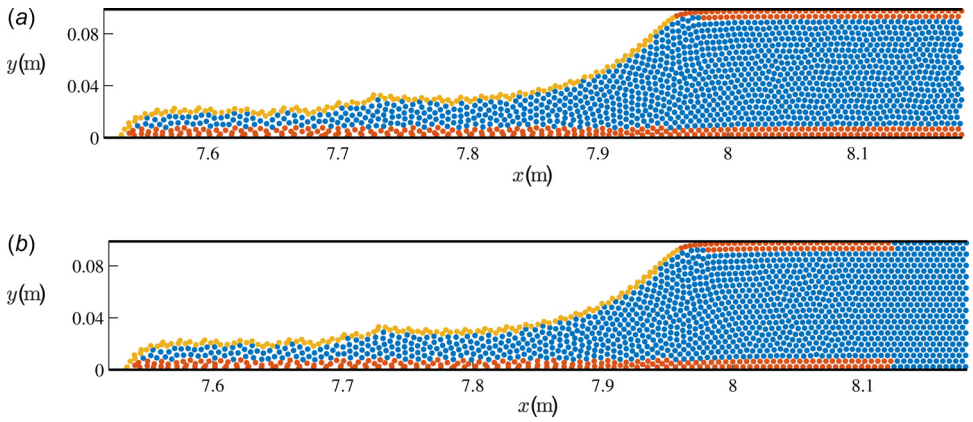

Fig. 2 Comparison of the tail of the slug at $t = 0.25$ s calculated with (*a*) the full simulation and (*b*) the hybrid model.

with S the set of particles that has been temporarily stored, as explained in Appendix A. Then, the accelerations tangent to the wall of all particles (also those in front and tail) are reduced per time step according to

$$\frac{\mathrm{d}u}{\mathrm{d}t} = -\frac{f}{2D}u_{\mathrm{avg}}^2 \tag{11}$$

Any additional friction, turbulence, or air-entrainment effects in front and tail have not been taken into account.

4 The Slug's Velocity and the Holdup Coefficient

We now compare our SPH results with those of the symbolic one-dimensional solutions given in Appendix B. To that end, we simulate an initially block-shaped liquid slug with length $L_0 = 1$ m in a horizontal pipe with diameter $D = 0.01$ m. Gravity is included, as well as wall friction with $f = 0.0$[illegible]. The initial particle distance is $d = 5 \times 10^{-4}$ m, resulting in [illegible]23 particles. In the early stages of the simulation, the hybrid model reduces the number of particles to just 1564. The density of the fluid is $\rho = 1000\,\mathrm{kg/m^3}$. In Eq. (6), we use the Wendland kernel

$$K_{ij} = K\left(|\mathbf{q}|, \tilde{h}\right) = \frac{7}{\pi \tilde{h}^2}(1 - |\mathbf{q}|)_+^4(4|\mathbf{q}| + 1) \tag{12}$$

where $(\cdot)_+ := \max(0, \cdot)$, $\mathbf{q} := (\mathbf{x}_i - \mathbf{x}_j)/\tilde{h}$, and $\tilde{h} = \sqrt{(18/5)}h$ is the radius of the support domain, with smoothing length $h = 1.5d$.

4.1 The Velocity of the Slug's Front. During the computations, we keep track of the average horizontal velocity of all the particles that constitute the free surface at the slug's front. We consider two cases: in case one, $P = 10^5$ Pa and $\Delta t = 10^{-5}$ s, while in case two, $P = 10^6$ Pa and $\Delta t = 5 \times 10^{-6}$ s. The velocity histories of the slug's front in both cases are shown in Fig. 4, together with one-dimensional solutions. The one-dimensional model is sketched in Fig. 5(*a*). The holdup coefficient β is defined as the holdup area divided by the conduit area. For a rectangular cross section, $\beta = H/D$ (Fig. 5(*b*)).

Initially, the results of the SPH simulation are almost identical to those of the one-dimensional solution without holdup ($\beta = 0$). This might be expected, because the effect of holdup on the slug's acceleration is proportional to u^2 and therefore small in the beginning. Soon, however, the holdup starts to have effect. After the slug has traveled about twice its own initial length, the difference between the SPH simulation and the one-dimensional model without holdup becomes visible.

Figure 4 also shows the velocity profiles given by the one-dimensional model with holdup for several values of β. Clearly, the one-dimensional models are able to predict the shape of the slug's velocity profile very well. More specifically, in the case $P = 10^5$ Pa, we find that if we choose $\beta = 0.0415$, the predicted velocity profile of the one-dimensional model is in very close agreement with that of our two-dimensional simulation. In the case $P = 10^6$ Pa, accurate predictions are found when $\beta = 0.044$ (not shown in Fig. 4(*b*)) and $\beta = 0.043$.

4.2 The Holdup Coefficient in Relation With the Slug's Length. The unknown value for β that should be used in the one-dimensional model can be extracted from the SPH simulation. To that end, we keep track of the length of the inner slug, which we define as the horizontal distance between the two flow-separation

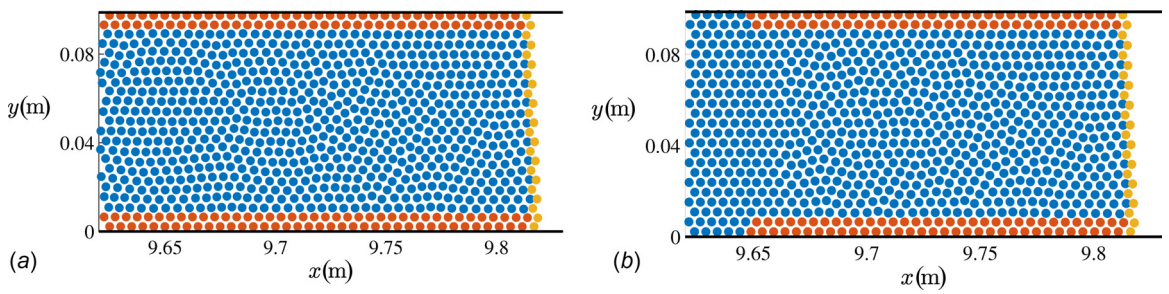

Fig. 3 Comparison of the front of the slug at $t = 0.25$ s calculated with (*a*) the full simulation and (*b*) the hybrid model.

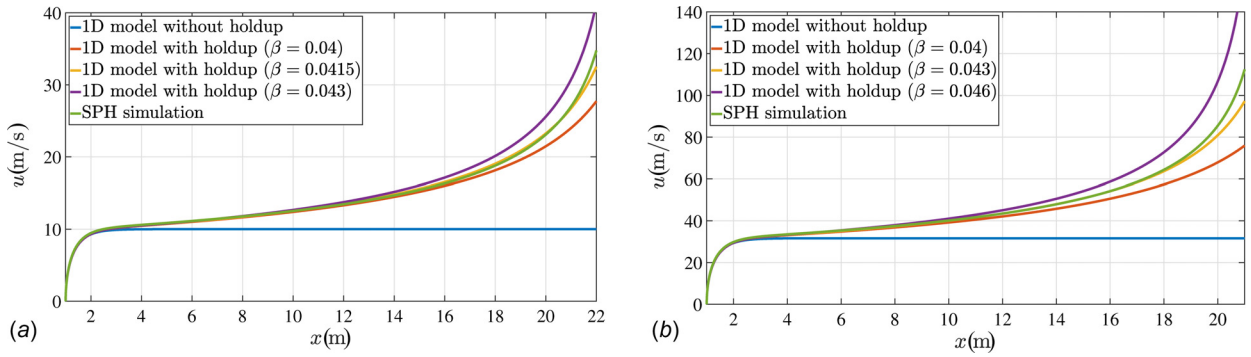

Fig. 4 The slug's front velocity as a function of its position when (*a*) $P = 10^5$ Pa and (*b*) $P = 10^6$ Pa. Comparison between the SPH simulation and the one-dimensional models without ($\beta = 0$) and with holdup.

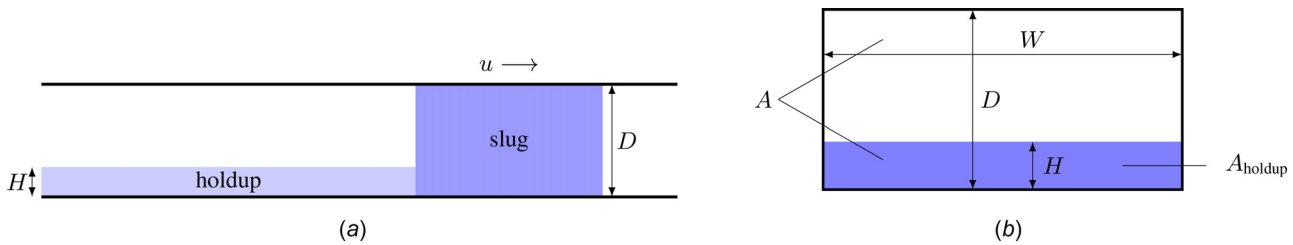

Fig. 5 Illustration of the one-dimensional models with holdup, as in Ref. [20]

points at the top of the conduit. This length is shown in Fig. 6(*a*), together with a linear fit of the data.

From the definition of the slug length L in Eq. (B3) in Appendix B, we derive that the slope s of the curves in Fig. 6(*a*) is related to the holdup coefficient in the following way:

$$s = -\frac{\beta}{1-\beta} \qquad \text{or} \qquad \beta = \frac{s}{s-1} \tag{13}$$

We approximate the slope of the curve corresponding to $P = 10^6$ Pa in Fig. 6(*a*) by means of a first-order finite difference scheme. Through Eq. (13), this leads to an approximation for the holdup coefficient β, which is depicted in Fig. 6(*b*). Apart from the peaky behavior, the result seems to suggest that β is constant in time.

If we use the slope of the linear fit we find that $\beta \approx 0.044$ (horizontal line in Fig. 6(*b*)), which agrees well with the results of the velocity profiles in Fig. 4(*b*). Thus, we may conclude that the assumption of a constant holdup coefficient is very reasonable indeed.

4.3 The Holdup Coefficient in Relation With the Slug's Tail. The holdup coefficient b in a rectangular conduit is the ratio of the depth H of the holdup and the height D of the slug (Fig. 5(*b*)). As such, we are able to approximate its value from the SPH simulation by computing the average depth of the slug's tail (the holdup). To that end, we count the number of particles left of the left flow-separation point (this is the point where the inner slug feels the driving pressure P; the pressure gradient in the tail is small). This number is multiplied by the volume of a single particle and divided by the horizontal length of the slug's tail (distance from the outer left particle to the left flow-separation point). This gives an estimate for β, which for the case in which $P = 10^6$ Pa is shown in Fig. 6(*b*).

When the traveled distance is small, there is little or no holdup. Therefore, the results for small values of x are unreliable and of less importance, because holdup does not influence the slug's velocity initially. After that, for distances between 4 m and 22 m, the values of the holdup coefficient converge to $\beta \approx 0.040$. Again, this supports the assumption of a constant holdup coefficient, albeit with a slightly smaller value. Recall that with the one-dimensional model the most accurate predictions are found when

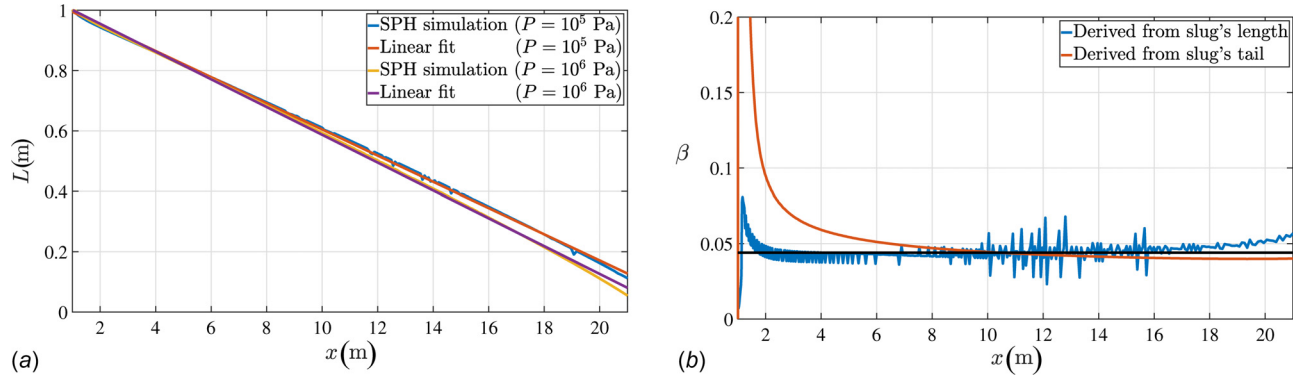

Fig. 6 (*a*) the slug's length as a function of its front position for both $P = 10^5$ Pa and $P = 10^6$ Pa and (*b*) the values of β derived from the SPH simulation for $P = 10^6$ Pa, where the black line indicates $\beta = 0.044$

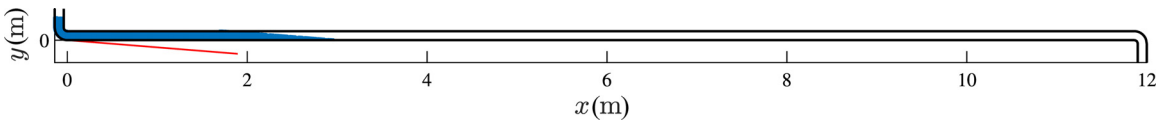

Fig. 7 Setup of the numerical simulations. The tilted line is the horizontal and indicates the angle of inclination.

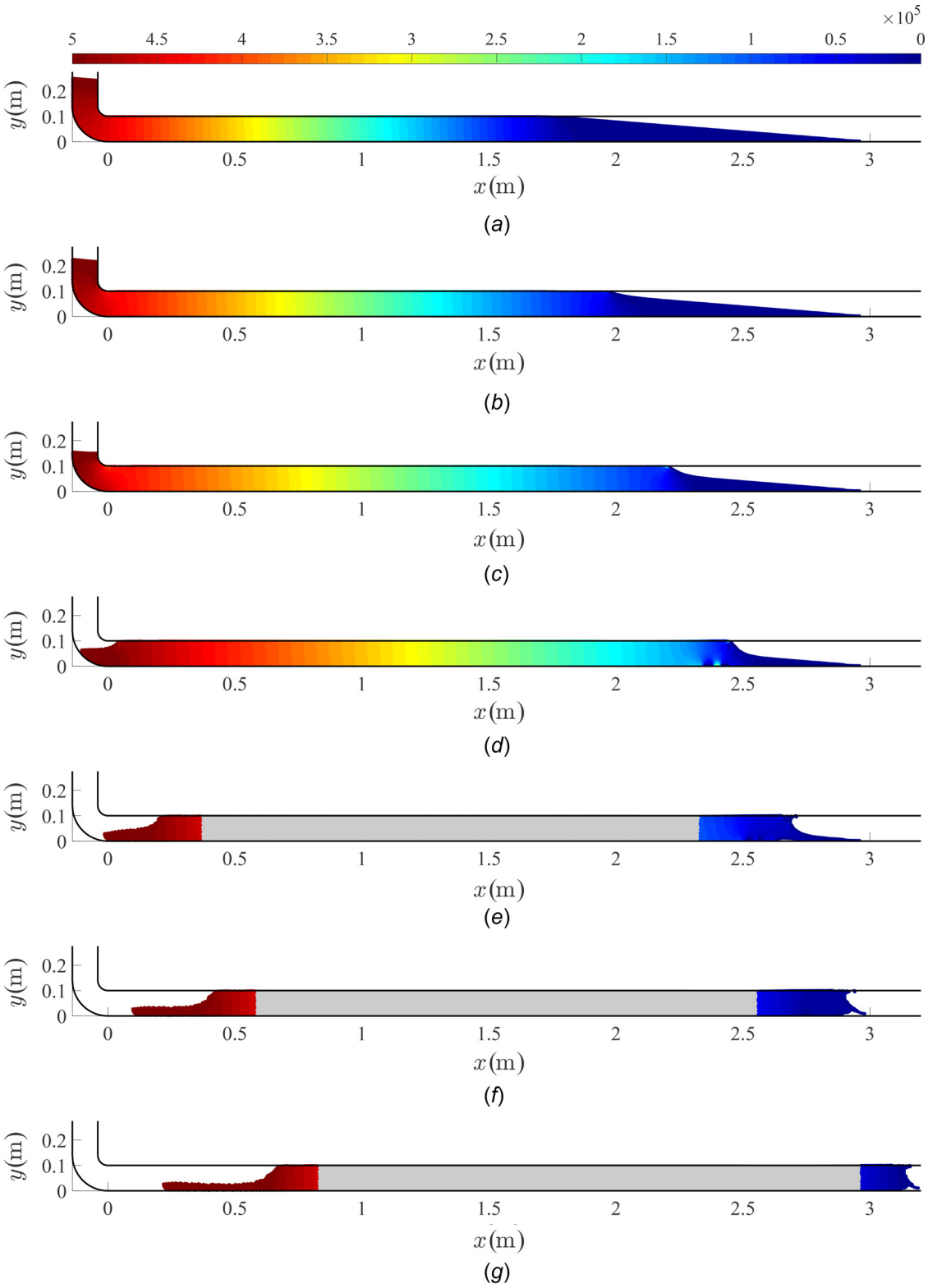

Fig. 8 Simulation of a traveling liquid slug starting from rest in an inclined pipe, showing the pressure distribution in the slug. In Figures (*e*), (*f*) and (*g*) the slug is fully contained in the straight section of the pipe and the hybrid model is applied.

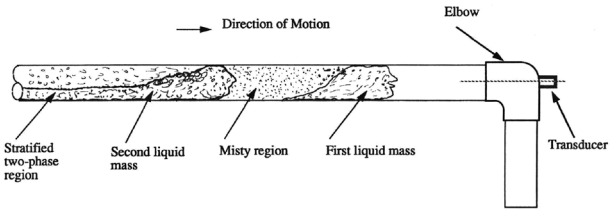

Fig. 9 Representation of the observed slug flow pattern by Bozkuş and Wiggert [7]

$\beta = 0.043$ or 0.044, which is close to the currently estimated value of 0.040.

5 Accelerating Liquid Slugs in an Inclined Pipe

In our simulations, we consider the experiments by Bozkuş et al. [9] on a pipe with diameter $D = 0.1$ m. The main pipe is 12 m long and has an upward slope of $\theta = 0.08$ radians (see Fig. 7). In our first simulation, the slug has an initial length of $L_0 = 3$ m. The initial particle spacing is chosen as $d = 0.006$ m, leading to 11,975

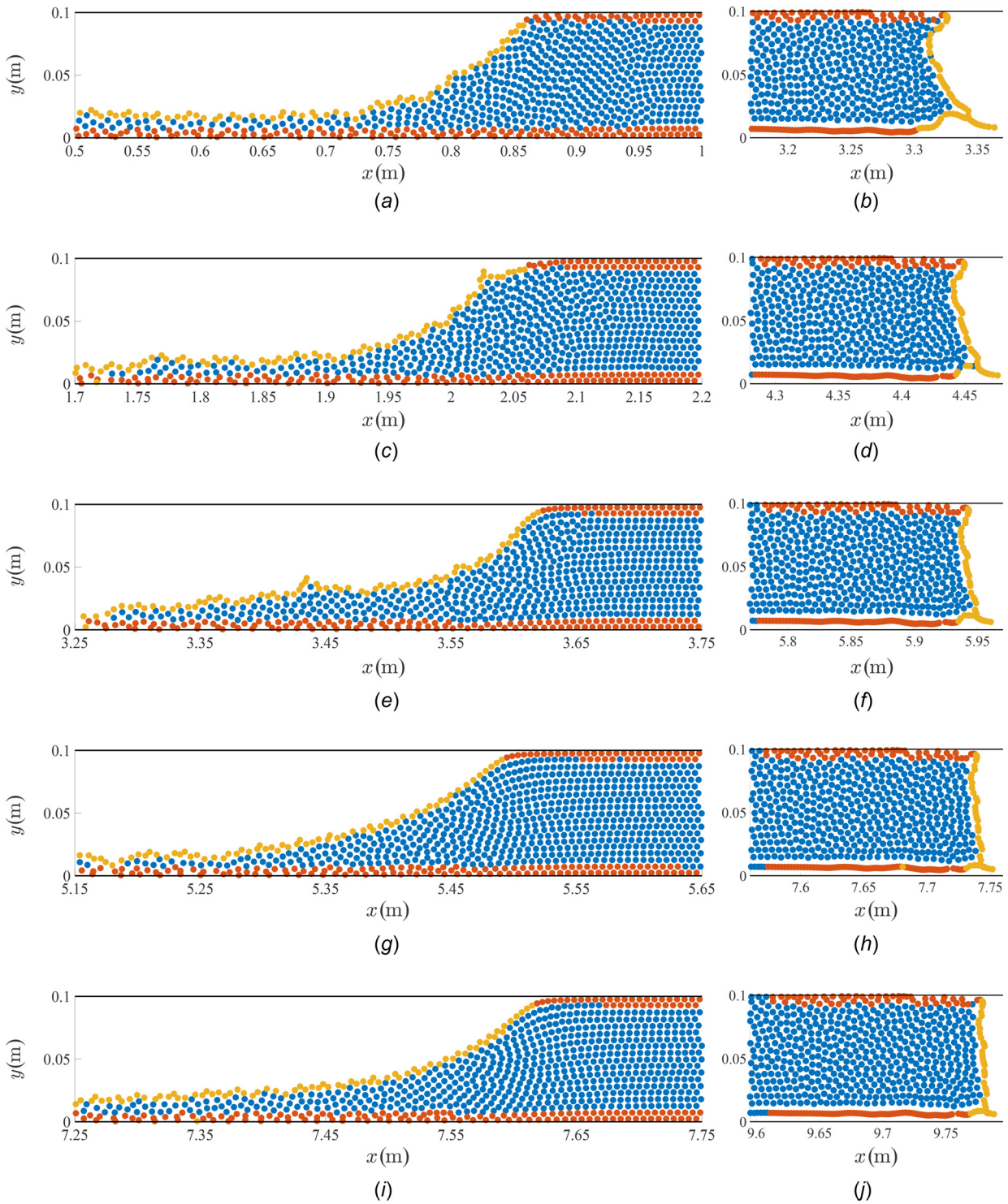

Fig. 10 Simulation of a traveling liquid slug in an inclined pipe.

particles. Both the downstream and upstream bend have a smooth, circular shape in the simulation (at the moment we are not able to correctly simulate the impact on a square bend; possible reasons are the geometric discontinuity and the incompressible liquid resulting in infinite accelerations). A sudden pressure $P = 500{,}000\,\text{Pa}$ is exerted from the left, as illustrated in Fig. 1. This induces a pressure distribution as shown in Fig. 8(*a*).

The early stages of the simulated slug motion are shown in Fig. 8. Here, $\Delta t = 10^{-5}$ s. The liquid slug is gently pushed through the lower bend. When the slug has just passed around the corner, the

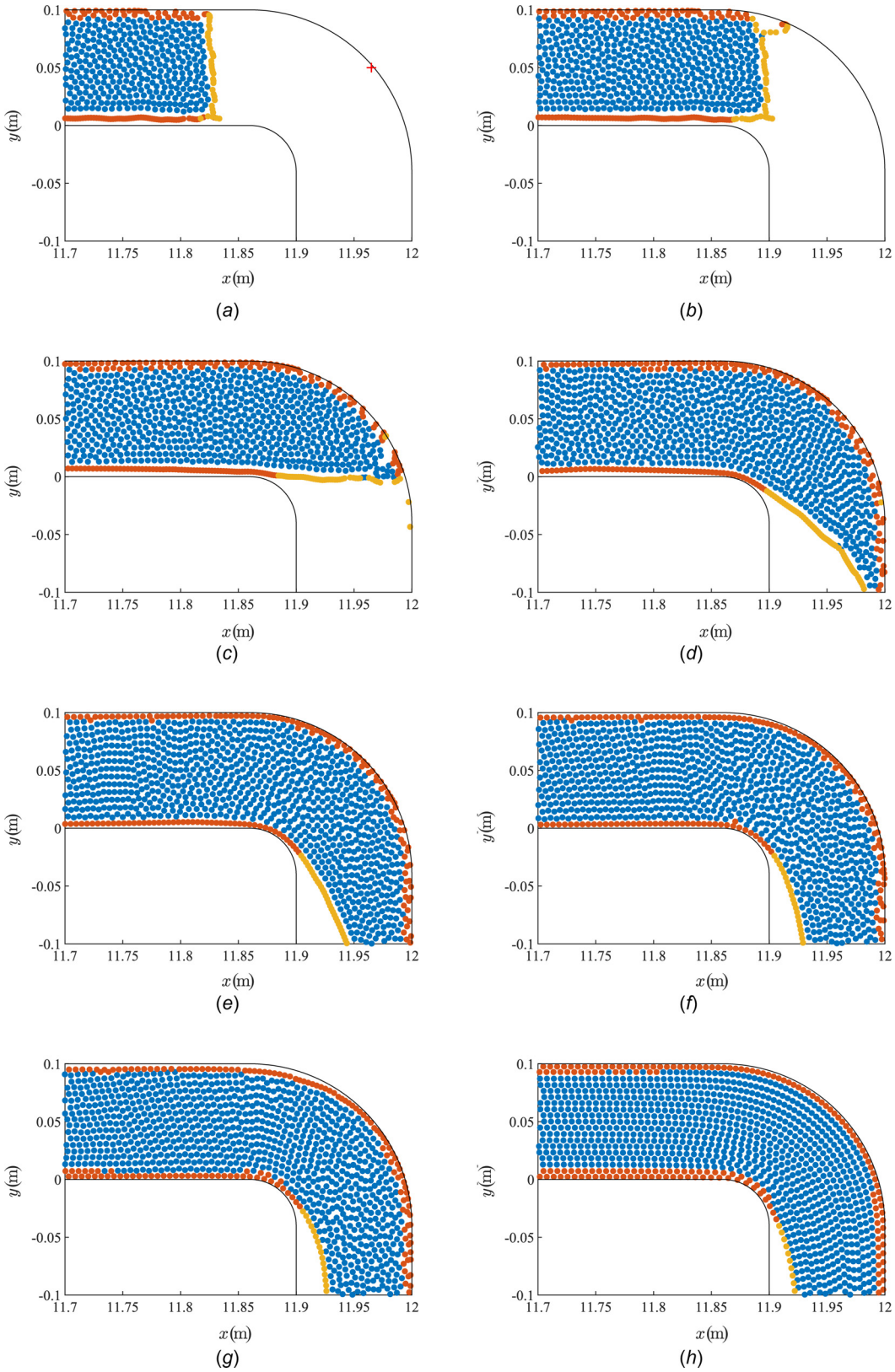

Fig. 11 Simulation of a liquid slug hitting and passing an elbow. The cross in (*a*) indicates the position of the monitor point.

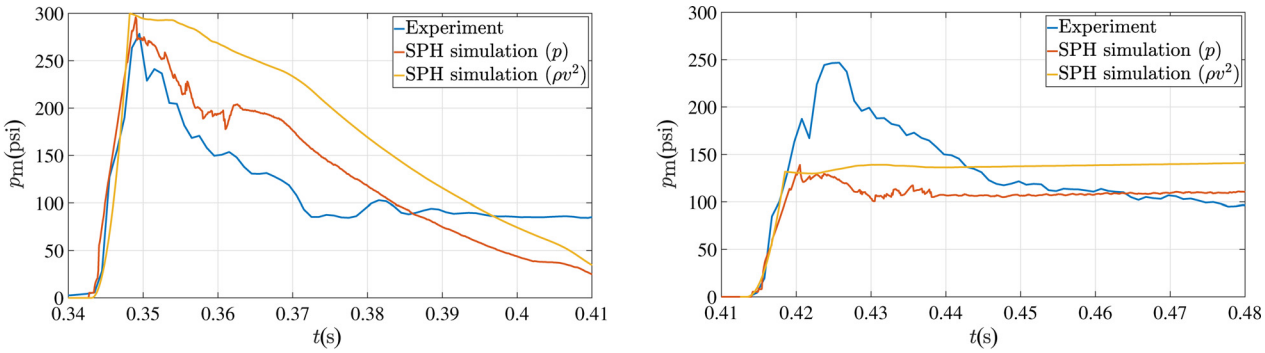

Fig. 12 The gauge pressure exerted by the liquid slug on the downstream bend in an inclined pipe when (*a*) $L_0 = 3$ *m* and (*b*) $L_0 = 5$ m. A comparison of our SPH simulation with the measurement of Bozkuş et al. [9]. Note: 100 psi ≈ 7 bar.

upper layer of the slug is already accelerating faster than the bottom layer. This results in an overshoot of the upper layer at the front of the slug, which is visible in Fig. 8(*e*). The overshoot is "pulled on" by gravity, so that over time the slug's front becomes steep and finally nearly planar. An opposite effect occurs at the slug's tail. There, the higher acceleration of the top layer increases the dam-break mechanism of gravity, so that the slug's tail gradually forms the holdup.

When the top layer of the slug overtakes the bottom layer, a protuberance is created at the bottom of the slug's front (see Fig. 8(*f*)). This makes the front look very similar to the one observed in reality in Ref. [7] and which is shown in Fig. 9. The protuberance is a result attributed to the small inclination angle, because it does not (or less) appear when θ is larger. Notice that in Figs. 8(*e*)–8(*g*), the entire slug is contained in the straight section of the pipe, and therefore, the hybrid model is applied, with an assumed linear pressure distribution in the inner slug.

Figure 10 shows the slug's front and tail at later stages of the simulation. Over time, the slug's tail becomes a bit smoother. The protuberance at the front of the slug becomes less apparent (see Figs. 10(*b*)–10(*j*)).

When the slug reaches the elbow at the end of the main pipe, it has an inner length of approximately 2.1 m and a velocity of 46 m/s. By this time, the protuberance has almost disappeared completely and the front is nearly planar (see Fig. 11(*a*)). The slug travels through the bend quite gently, especially sometime after the impact (see Fig. 11(*h*)).

The pressure force exerted by the slug on the bend is calculated at a monitor position $\mathbf{x}_m$ according to

$$\langle p_m \rangle = \sum_{j \in S_{\mathbf{x}_m}} p_j \, K(\mathbf{x}_m - \mathbf{x}_j, h) \, V_j \tag{14}$$

As for the measured signals in Ref. [9] (see Eq. (11) in that paper), we carry out a smoothing treatment (5 ms time average) to filter out any nonphysical oscillations

$$\langle p_m \rangle^n = \frac{1}{50} \sum_{i=n}^{n+49} \langle p_m \rangle^i \tag{15}$$

For $\mathbf{x}_m = (11.965, -0.09)$ m, the resulting pressure evolution is shown in Fig. 12(*a*). It also shows the pressure prediction based on the inner slug's horizontal velocity ($p = \rho u_{\text{avg}}^2$). We compare our results with the pressure history obtained experimentally by Bozkuş et al. [9]. Their results, for a slug of initial length $L_0 = 3$ m and a pressure of $P = 500{,}000$ Pa, are also given in Fig. 12(*a*). We find that the magnitude of the impact pressure is in very close agreement with that found experimentally. This implies that the impact velocity is correctly predicted. The pressure decay in our simulations is more or less constant, whereas in the experiments by Bozkuş et al. [9], it decreases faster immediately after the impact and slower at later stages. To determine what causes this difference, more (experimental) results are needed, in particular photographic or video images. The ρu_{avg}^2 -result gives an acceptable conservative prediction.

In a second simulation, the slug has an initial length of $L_0 = 5$ m. Other parameters are the same as before, including the initial particle spacing, so that we start with 15,577 particles. We find that the behavior of the slug during the early stages of the acceleration, as

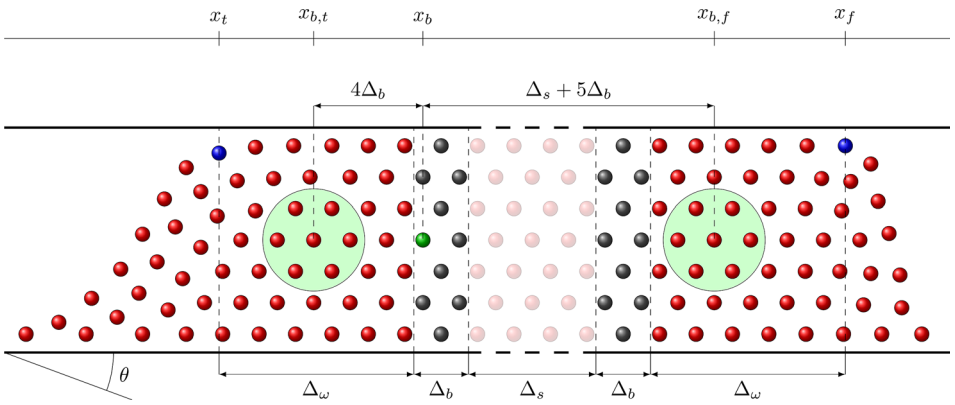

Fig. 13 The front (right) and tail (left) of the slug are simulated with two-dimensional SPH. The middle part is replaced by a quasi two-dimensional model.

well as in the straight section of the pipe, is similar to the behavior of the shorter slug in the first simulation. At the time of impact, the slug has an inner length of approximately 4.5 m and a velocity of 30 m/s. The calculated impact pressure exerted by the slug on the upper bend is lower and different than in the previous case, as shown in Fig. 12(*b*). After the impact, the exerted force on the bend stays on the same level. Intuitively this seems correct, as the slug is still traveling at nearly constant speed through the bend, but it does not agree with the experimental results of Bozkuş et al. [9], which show a nearly two times higher pressure peak and a gradual decay. The analytical one-dimensional model predicts an impact velocity similar to that in our SPH simulations [20], which suggests that for long slugs there is something wrong in either the experiment or our model assumptions. For example, an entrapped air pocket may occur in the upper corner of the elbow.

6 Conclusions

In this paper, we simulated liquid slugs traveling in void pipelines. To that end, we adopted the incompressible SPH method. We introduced a hybrid model that enabled us to leave out the larger inner part of the slug. This saved a significant amount of computational time, depending on the slug's length. Furthermore, a higher resolution could be achieved in the slug's front and tail. The hybrid model had no adverse effect on the shapes of the slug's front and tail.

We validated our simulation results against laboratory measurements. The steep front and the smooth tail of the slugs found in our simulations were consistent with the shapes found by Bozkuş and Wiggert [7]. Also, the slug's speeds and the pressure force exerted by the short slugs on bends were consistent with the results obtained experimentally by Bozkuş et al. [9]. For long slugs, peak pressures were underestimated.

We also validated our results against the analytical, one-dimensional model of Tijsseling et al. [20]. It was found that the impact velocities predicted by our simulations were consistent with the velocities given by the analytical model.

Finally, we studied the one-dimensional model of Tijsseling et al. [20] and the unknown holdup-coefficient β that they use. We found that their assumption of a constant holdup coefficient is a valid one. More specifically, we found that the predictions of the one-dimensional model with $0.041 \leq \beta \leq 0.044$ were in very close agreement with our two-dimensional SPH results.

Acknowledgment

The authors would like to thank the reviewers for their helpful comments.

Funding Data

- Nederlandse Organisatie voor Wetenschappelijk Onderzoek (NWO) VICI Grant No. 639.033.008.

Appendix A: The Hybrid Model

The hybrid model is implemented as follows. First, we look for the flow separation points (left and right top corners of the inner slug). Before the hybrid model is applied, the free surface particles have already been identified through the procedure described in Ref. [23]. We now consider the particles constituting the left free surface. The left flow separation point is then indicated by the position of the particle with the largest x-coordinate. A similar procedure is followed to find the right flow separation point. Both particles are at the top at x_t and x_f, respectively, in Fig. 13. Let us denote the axial locations of these particles by x_t (tail) and x_f (front). Then, all particles s for which

$$x_t + (\Delta_\omega + \Delta_b) < x_s < x_f - (\Delta_\omega + \Delta_b) \tag{A1}$$

are temporarily removed from the SPH simulation. We denote this set of particles by S. The value of Δ_ω should be chosen such that at a distance Δ_ω from the separation points the effects of the free surface are negligible. The distance Δ_b is used to define a thin layer in which particles will act as boundary particles. In our computations, we used $\Delta_\omega = 20\,h$ and $\Delta_b = 2\,h$, but other values may be used as well. The separated inner part always has height D, while its length Δ_s is adapted every time step. It may be very long relative to D, as indicated by the bold dashed lines representing the walls in Fig. 13. The particle-removal step is performed at the beginning of a time step, even before the computation of the auxiliary velocities.

By removing the particles in S we are left with two separate parts of the slug: the front and the tail. This introduces two more boundaries: right from the tail and left from the front. To solve Eq. (5), we need to know which particles constitute these boundaries. In general, these particles will not be positioned on straight vertical lines. Therefore, we introduce boundary areas, with all particles b for which

$$x_t + \Delta_\omega < x_b < x_t + \Delta_\omega + \Delta_b \quad \text{or} \quad x_f - \Delta_\omega - \Delta_b < x_b < x_f - \Delta_\omega \tag{A2}$$

designated as boundary particles. The set containing these particles is denoted by $B = B_t \cup B_f$ (with B_t and B_f containing the particles of B located in the tail and front of the slug, respectively). These boundary particles will impose the necessary boundary conditions on Eq. (5), in addition to the existing set of boundary conditions for rigid walls and free surfaces. To that end, we select two axial positions for every particle b. For instance, if $b \in B_t$, one point is located at $x_{b,t} = x_b - 4\Delta_b$ and the other—at the front of the slug—at $x_{b,f} = x_b + \Delta_s + 5\Delta_b$ (while $y_{b,t} = y_{b,f} = y_b$). This is illustrated for a particle in B_t in Fig. 13.

Now we use our assumption that the pressure in the inner part of the slug (taken from x_t to x_f) decreases linearly in the axial direction. With particle $b \in B_t$ located exactly on the line between $x_{b,t}$ and $x_{b,f}$, the pressure p_b at x_b is

$$\begin{aligned} p_b &\approx p_{b,t} + \frac{p_{b,f} - p_{b,t}}{|x_{b,f} - x_{b,t}|}\,|x_b - x_{b,t}| \\ &= p_{b,t} + \frac{p_{b,f} - p_{b,t}}{\Delta_s + 9\Delta_b}\,4\Delta_b, \end{aligned} \tag{A3}$$

where $p_{b,t}$ and $p_{b,f}$ are the (still unknown) pressures at the left and right selected points, respectively. We could approximate these pressures by the pressures of the nearest particles, but we choose to approximate it in a typical SPH way. Using

$$\langle f(\mathbf{x}) \rangle := \sum_{j \in S_\mathbf{x}} f(\mathbf{x}_j)\, K(\mathbf{x} - \mathbf{x}_j, h)\, V_j \tag{A4}$$

we calculate an average pressure $\langle p_{b,t} \rangle$ at $x_{b,t}$ in terms of the pressures of surrounding particles

$$\langle p_{b,t} \rangle = \sum_{j \in S_{\mathbf{x}_{b,t}}} p_j\, K(\mathbf{x}_{b,t} - \mathbf{x}_j, h)\, V_j \tag{A5}$$

with an analogous expression for $\langle p_{b,f} \rangle$. This step is illustrated by the circular support domains in Fig. 13. The final expression for the pressure at x_b (with $b \in B_t$) then reads

$$p_b \approx \langle p_{b,t} \rangle + \frac{\langle p_{b,f} \rangle - \langle p_{b,t} \rangle}{\Delta_s + 9\Delta_b}\,4\Delta_b \tag{A6}$$

Thus, we have written the pressure for a boundary particle b in terms of the pressures of internal fluid particles. In that sense, Eq. (A6) is used to enforce Neumann-like boundary conditions (depending on many particles instead of just one), which are added to the existing set of boundary conditions for Eq. (5). The devised procedure explained earlier ensures that the pressures of

the particles in the front and tail are directly connected. This makes the inner part of the slug (the Δs-area) redundant, and it can therefore be left out of the computations.

In the simulation with the hybrid model, we see particles getting a bit close to each other in the top part of the slug (see Fig. 3(*b*)), at the interface between the inner slug and the front part. This indicates that the inner part is moving slightly faster than the front part, which implies that the slug's tail is moving faster than its front. However, the extent to which this happens is very small [22], so that the model satisfactorily preserves volume.

After the pressures, accelerations, and new velocities and positions of the particles constituting the slug's front and tail have been computed, the inner slug's particles are reintroduced into the computations. The new velocities of these particles are unknown, since they were left out of the computations. Therefore, their new velocities are computed as follows. For the boundary particles $b \in B_t$, a linear relation is assumed between the horizontal velocities and the y-coordinates of the particles

$$u_b^{n+1} = \eta_t y_b^{n+1} + \zeta_t \quad \text{for} \quad b \in B_t \tag{A7}$$

The coefficients η_t and ζ_t are found from the two particles in B_t with the smallest and largest y-coordinate and their respective horizontal velocities u. The same procedure is then performed for the boundary particles in B_f. The horizontal velocities of the inner slug's particles are then computed as

$$u_s^{n+1} = \eta y_s^n + \zeta \quad \text{for} \quad s \in S \tag{A8}$$

where $\eta = (1/2)(\eta_t + \eta_f)$ and $\zeta = (1/2)(\zeta_t + \zeta_f)$. The vertical velocities v are set to zero in the quasi two-dimensional model

$$v_s^{n+1} = 0 \quad \text{for} \quad s \in S \tag{A9}$$

These velocities are then used to update the inner particle positions according to Eq. (8).

Appendix B: One-Dimensional Model

The one-dimensional model derived by Tijsseling et al. [20] is summarized. Assuming that the conduit is horizontal, the slug has no initial velocity, no force is exerted at its front, and no liquid is left behind (no holdup), they find that the velocity of the slug is given by

$$u(t) = u_\infty \tanh(\sqrt{C_1 C_2}\, t) \tag{B1}$$

where $C_1 := P/(\rho L_0), C_2 := f/(2D)$, and $u_\infty = u(\infty) = \sqrt{C_1/C_2}$. Recall that P is the magnitude of the driving pressure and L_0 is the (initial) length of the slug.

Tijsseling et al. [20] also considered the case in which liquid is left behind (see Fig. 5(*a*)). To that end, they introduced the holdup coefficient β, defined such that the cross-sectional area of the stationary liquid layer that is left behind is $A_{\text{holdup}} = \beta A$, where A is the cross-sectional area of the conduit (and the liquid slug). The velocity of the front of the slug can then be expressed in terms of incomplete gamma functions as

$$u(L) = e^{f^* L} \sqrt{\frac{\Gamma(\alpha, 2Lf^*)}{(2Lf^*)^\alpha} - \frac{\Gamma(\alpha, 2L_0 f^*)}{(2L_0 f^*)^\alpha} \left(\frac{L_0}{L}\right)^\alpha} \sqrt{2 \frac{(1-\beta)^2}{\beta\left(1-\frac{1}{2}\beta\right)} \frac{P}{\rho}} \tag{B2}$$

where

$$\alpha := 2\frac{1-\beta}{1-\frac{1}{2}\beta}, \quad f^* := \frac{f}{2D} \frac{1-\beta+\frac{1}{3}\beta^2}{\beta-\frac{1}{2}\beta^2}, \quad \text{and} \quad L = L_0 - \frac{\beta}{1-\beta} L_{\text{pipe}} \tag{B3}$$

In their notation, L_{pipe} is the distance traveled by the slug's front. If the incomplete gamma functions have very small values (close to machine precision), they are replaced by the leading term of their asymptotic expansions, so that Eq. (B2) becomes

$$u(L) = \sqrt{1 - \left(\frac{L_0}{L}\right)^{\alpha-1} e^{-2(L_0 - L)f^*}} \sqrt{\frac{(1-\beta)^2}{\beta\left(1-\frac{1}{2}\beta\right)} \frac{P}{\rho L f^*}} \tag{B4}$$

The holdup coefficient β relates the cross-sectional area of the liquid slug, A, to that of the holdup, A_{holdup}. Because in our simulations, we consider the vertical midplane of the pipe in which the slug moves, we prefer to relate the height of the slug D to the depth of the holdup H. For a rectangular conduit of width W and height H, as illustrated in Fig. 5(*b*), this relation simply is

$$\beta = \frac{H}{D} \tag{B5}$$

References

[1] Tijsseling, A., Hou, Q., Bozkuş, Z., and Laanearu, J., 2016, "Improved One-Dimensional Models for Rapid Emptying and Filling of Pipelines," ASME J. Pressure Vessel Technol., **138**(3), p. 031301.

[2] Kirsner, W., 1999, "Condensation-Induced Waterhammer," HPAC Heating/Piping/AirConditioning, **71**(1), pp. 112–122.

[3] Galante, C., and Pointer, S., 2002, "Catastrophic Water Hammer in a Steam Dead Leg," IChemE Loss Prevention Bull., **167**(1), pp. 16–20.

[4] Kirsner, W., 2005, "Condensation-Induced Water Hammer in District Steam Systems—Circumstances Resulting in Catastrophic Failures," ASME Paper No. PVP2005-71590.

[5] Carlson, M., 2011, "Condensation Induced Water Hammer and Steam Assisted Gravity Drainage in the Athabasca Oil Sands," 14th International Topical Meeting on Nuclear Reactor Thermal Hydraulics, Toronto, ON, Canada, Sept. 25–30, Paper No. NURETH14-600.

[6] Vecchio, R., Sinha, S., Bruck, P., Esselman, T., Zysk, G., and Somrah, D., 2015, "The 2007 New York City Steam Explosion: Post-Accident Analysis," 12th International Conference on Pressure Surges, Dublin, Ireland, Nov. 18–20, pp. 7–17.

[7] Bozkuş, Z., and Wiggert, D., 1997, "Liquid Slug Motion in a Voided Line," J. Fluids Struct., **11**(8), pp. 947–963.

[8] Martin, C., 2003, "Condensation-Induced Water Hammer in Horizontal Refrigerant Pipe With Warm Gas Entry," ASME Paper No. FEDSM2003-45678.

[9] Bozkuş, Z., Baran, O., and Ger, M., 2004, "Experimental and Numerical Analysis of Transient Liquid Slug Motion in a Voided Line," ASME J. Pressure Vessel Technol., **126**(2), pp. 241–249.

[10] Prasser, H., Ézsöl, G., Baranyai, G., and Sühnel, T., 2008, "Spontaneous Water Hammers in a Steam Line in the Case of Cold Water Ingress," Multiphase Sci. Technol., **20**(3–4), pp. 265–290.

[11] Martin, C., 2013, "Waterhammer in a Horizontal Pipe Induced by Slug Formation and Rapid Condensation," ASME Paper No. PVP2013-97424.

[12] Dirndorfer, S., Kulisch, H., and Malcherek, A., 2013, "Experiments of Condensation-Induced Water Hammers at the UniBw Munich," Kerntechnik, **78**(1), pp. 22–24.

[13] Barna, I., Imre, A., Baranyai, G., and Ézsöl, G., 2010, "Experimental and Theoretical Study of Steam Condensation Induced Water Hammer Phenomena," Nucl. Eng. Des., **240**(1), pp. 146–150.

[14] Barrera, C., and Kemal, A., 2010, "Condensation Induced Water Hammer: Principles and Consequences," AIChE Spring Meeting and Sixth Global Congress on Process Safety, San Antonio, TX, Mar. 22–24, pp. 719–731.

[15] Xing, L., Yeung, H., and Lo, S., 2011, "Investigation of Slug Flow Induced Forces on Pipe Bends Applying STAR-OLGA Coupling," 15th International Conference on Multiphase Production Technology, Cannes, France, June 15, pp. 327–344.

[16] Swidersky, H., 2013, "Condensation Induced Water Hammer (CIWH)—Relevance in the Nuclear Industry and State of Science and Technology," Kerntechnik, **78**(1), pp. 16–21.

[17] Blömeling, F., Neuhaus, T., and Schaffrath, A., 2013, "1D Models for Condensation Induced Water Hammer in Pipelines," Kerntechnik, **78**(1), pp. 31–34.

[18] Hou, Q., Tijsseling, A., and Bozkuş, Z., 2014, "Dynamic Force on an Elbow Caused by a Traveling Liquid Slug," ASME J. Pressure Vessel Technol., **136**(3), p. 031302.

[19] Barna, I., Pocsai, M., Guba, A., and Imre, A., 2015, "Theoretical Study of Steam Condensation Induced Water Hammer Phenomena in Horizontal Pipelines," Kerntechnik, **80**(5), pp. 420–423.

[20] Tijsseling, A., Hou, Q., and Bozkuş, Z., 2016, "An Improved One-Dimensional Model for Liquid Slugs Traveling in Pipelines," ASME J. Pressure Vessel Technol., **138**(1), p. 011301.

[21] Tay, B., and Thorpe, R., 2014, "Hydrodynamic Forces Acting on Pipe Bends in Gas-Liquid Slug Flow," Chem. Eng. Res. Des., **92**(5), pp. 812–825.

[22] Korzilius, S., 2016, "Second Derivatives, Particle Collisions and Travelling Liquid Slugs Within Smoothed Particle Hydrodynamics," Ph.D. thesis, Eindhoven University of Technology, Eindhoven, The Netherlands.

[23] Marrone, S., Colagrossi, A., Le Touzé, D., and Graziani, G., 2010, "Fast Free-Surface Detection and Level-Set Function Definition in SPH Solvers," J. Comput. Phys., **229**(10), pp. 3652–3663.